



Semnan University

Mechanics of Advanced Composite Structures

journal homepage: <http://MACS.journals.semnan.ac.ir>

Vibration of MEE Composite Conical Shell Surrounded by Nonlinear Elastic Foundation Considering the Effect of Geometrical Nonlinearity

S. Mohammadrezazadeh

Faculty of Mechanical Engineering, K. N. Toosi University of Technology, Tehran, 1991943344, Iran

KEYWORDS

MEE composite conical shell;
Geometrical nonlinearity;
Nonlinear elastic foundation;
Lagrange method;
Lindstedt-Poincare method.

ABSTRACT

This paper is investigated vibration of magneto-electro-elastic (MEE) composite conical shell on a nonlinear elastic foundation and under electric or magnetic potential while the influence of geometrical nonlinearity is taken into account. The conical shell is modeled based on the von Karman approach while the influences of shear deformation and rotary inertia are heeded. Coupled relations of MEE material are utilized to derive the vectors of stress, electric displacement as well as magnetic induction. Quasi-static Maxwell equations, Gauss' laws as well as thin shell assumptions are used to determine electric and magnetic fields. The nonlinear ordinary differential equation of the shell is derived through the Lagrange approach. Lindstedt-Poincare method and modal analysis are hired in order to obtain nonlinear vibration responses of the MEE composite conical shell. For validation intention, some results of the literature are compared with some results of this study. The effects of several parameters including nonlinear and linear constants of foundation, electric and magnetic potentials, thickness as well as length on the values of fundamental linear frequency, nonlinear parameter, and the curves of nonlinear frequency ratio versus amplitude parameter are investigated. The results show that the increase of the nonlinear constant of elastic foundation or thickness causes the increase of the nonlinear frequency ratio. On the other hand, the nonlinear frequency ratio gets smaller values with an increase in the linear constants of the elastic foundation or length.

1. Introduction

Structural mechanics is one of the interesting topics considered in numerous researches [1-11]. In addition, several studies considered nano-scale structures [12-15]. Furthermore, an example of a study on the micro-scale is the study that was done by Ouakad and ŽUR [16]. The focus of this study is on the vibration of conical shell structures on an elastic foundation composed of magneto-electro-elastic (MEE) material. Magneto-electro-elastic composite materials are smart materials that have the ability to convert magnetic, electrical, and mechanical energies to each other [17]. These materials can be used for actuators, sensors, and also vibration control purposes [17]. There are several works in literature that take attention to the study of structures containing magneto-electro-elastic

materials. Bhangale and Ganesan [18] studied the vibration of functionally graded magneto-electro-elastic cylindrical shells via a finite element model. Annigeri et al. [19] investigated the vibration behavior of a magneto-electro-elastic cylindrical shell subjected to simply supported boundary conditions using a series solution and finite element model. Tsai and Wu [20] presented three-dimensional free vibration responses of simply supported doubly curved shells composed of functionally graded magneto-electro-elastic material with open-circuit surface conditions via an asymptotic method. Kumaravel et al. [21] adopted the finite element method to study the vibration and buckling of magneto-electro-elastic cylinders under clamped-clamped boundary conditions. Lang and Xuewu [22] accomplished a study about the vibration and buckling of cylindrical shells from functionally

* Corresponding author. Tel.: +98-21-88674747 ; Fax: +98-21-88674748
E-mail address: sh.mrezazadeh@gmail.com

graded magneto-electro-thermo-elastic material by means of higher-order shear deformation theory. Razavi and Shoostari [17] carried out an investigation about the free vibration of simply supported thin magneto-electro-elastic doubly-curved shells surrounded by a foundation with the help of Donnell theory. Shoostari and Razavi [23] carried out the large amplitude vibration study of simply-supported magneto-electro-elastic curved panels on the basis of the Donnell shell theory and the Galerkin approach. Shoostari and Razavi [24] hired the Galerkin method and Lindstedt-Poincare perturbation approach to investigate linear and nonlinear vibration of magneto-electro-elastic laminated doubly-curved thin shell resting on an elastic foundation. Mohammadimehr et al. [25] utilized first-order shear deformation theory, energy method, and Hamilton principle to research the free vibration of magneto-electro-elastic composite cylindrical panels reinforced by carbon nanotubes considering closed and open circuit boundary conditions. Vinyas and Harursamphath [26] investigated nonlinear vibration of higher order shear deformable Carbon nanotube reinforced magneto-electro-elastic doubly curved shells on the basis of the Donnell shell theory and von-Karman nonlinear approach. Rostami and Mohammadimehr [27] dealt with the vibration control of a sandwich rotating cylindrical shell containing a nanocomposite face sheet and porous core and integrated with functionally graded magneto-electro-elastic layers applying differential quadrature method and first-order shear deformation theory of shells. Ye et al. [28] studied transient dynamic and free vibration of composite magneto-electro-elastic cylindrical shells via the scaled boundary finite element method. Rostami et al. [29] researched the vibration control of the sandwich rotating cylindrical shell which had functionally graded core and functionally graded magneto-electro-elastic layers on the basis of the first-order shear deformation theory of shells and differential quadrature method. Ni et al. [30] employed a Hamiltonian system to study the vibration of porous magneto-electro-thermo-elastic functionally graded cylindrical shells under magneto-electro-thermal loadings. Zhou et al. [31] obtained the time-dependent responses of MEE structures in a hygrothermal environment using the cell-based smoothed finite element technique in conjunction with the modified Newmark procedure. Farajpour et al. [32] studied large amplitude vibration of magneto-electromechanical mass nanosensors. The nanomechanical sensor utilized vibrating MEE nanoplates with numerous locations in order to trap nanoparticles [32]. It is obvious that

references [17] to [32] are not about the study of conical shells.

Conical shells are from engineering structures that have a lot of applications including piping, pressure vessels, and ship structures [33]. An investigation of the free vibration of magneto-electro-elastic conical shells under clamped-free, simply supported and clamped-clamped boundary conditions based on the finite element method was done by Srikantamurthy et al. [34]. In addition, Srikantamurthy and Annigeri [35] studied the free vibration of multiphase MagnetoElectro-Elastic uniform thickness conical shells under Clamped-Free boundary conditions. References [34] and [35] considered the vibration of MEE conical shells, but they did not study the vibration of MEE conical shells on elastic foundations.

Vibration characteristics of conical structures on linear elastic foundations were studied by many researchers [36-50]. It is necessary to mention that the behavior of the foundation is generally nonlinear [51]. The author found that there are limited papers in the literature about the vibration of conical structures on nonlinear elastic foundations. Zhu et al. [52] accomplished the smart control of large amplitude vibration of porous piezoelectric sandwich conical panels surrounded by nonlinear elastic foundation via first-order shear deformation theory, von Kármán nonlinear approach, and harmonic balance method. The considered conical panel contained a viscoelastic core as well as two porous piezoelectric layers [52]. Molla-Alipour et al. [53] studied free vibration of the bidirectional functionally graded cylindrical and conical shells as well as annular plates on nonlinear elastic foundations. References [52] and [53] investigated the vibration of conical structures on a nonlinear elastic foundation, but the conical structures are not from MEE material.

To the best of the author's knowledge, there is not any study in the literature which considers nonlinear vibration of simply supported MEE composite conical shells surrounded by the nonlinear elastic foundation. This study considers the nonlinear vibration responses of simply supported MEE composite conical shells on nonlinear elastic foundations subjected to electric or magnetic potential. The nonlinearity of the system is due to the geometric nonlinearity modeled via the von Karman approach as well as foundation nonlinearity. The effects of shear deformation as well as rotary inertia are taken into account in the process of shell modeling.

Unfortunately, it is not possible to obtain an exact solution for a great number of mathematical problems. Numerical methods are effective methods that are extremely used for the solution of mathematical problems. For example,

the discrete singular convolution method which is a numerical method is used in several researches such as [54-56]. Regardless of the advantages of the numerical methods, analytical methods are used in order to have parametric studies, consider the physics of problems and validate the numerical results [57-58]. In reference [59], a semi-analytical method was employed in order to solve equations. Because of the advantages of approximate analytical methods, in this study, the Lagrange method as an approximate analytical method is handled to convert the partial differential equations of the conical shell to an ordinary differential equation. Lindstedt-Poincare method and modal analysis are employed to obtain the nonlinear response of the system. Several results from published literature are compared with the results of this study for validation purposes. In the next step, the effects of several parameters including nonlinear and linear constants of elastic foundation, thickness, electric and magnetic potentials, thickness, and length on the fundamental linear frequency as well as nonlinear vibration responses are illustrated.

2. Modeling of the Shell

2.1. Strain Relations

Figure 1 shows the coordinate system and schematic of the considered MEE composite conical shell. In addition, a schematic of the conical shell on a nonlinear elastic foundation is depicted in Figure 2.

The longitudinal, circumferential, and normal directions of the coordinate system are shown

with x , θ and z , respectively. The variable L depicts the length, h is the thickness, α implies a semi-vertex angle and R_1 and R_2 are respectively the radii of small and large edges on the middle surface of the shell. The radius of each point on the middle surface of the shell is denoted by $R(x) = R_1 + x \sin \alpha$.

Equation (1) indicates the relations of strains $(\epsilon_x, \epsilon_\theta, \epsilon_{x\theta})$ with membrane strains $(\epsilon_{0x}, \epsilon_{0\theta}, \epsilon_{0x\theta})$ as well as curvatures $(k_x, k_\theta, k_{x\theta})$ [61]:

$$\epsilon_x = \epsilon_{0x} + zk_x, \epsilon_\theta = \epsilon_{0\theta} + zk_\theta, \epsilon_{x\theta} = \epsilon_{0x\theta} + zk_{x\theta} \quad (1)$$

Considering the von Karman approach for geometrical nonlinearity and shear deformation leads to equations (2) and (3) for membrane strains and curvatures, respectively [61-62]. In addition, shear strains in the middle surface of the conical shell are extracted through equation (4) [61]:

$$\begin{aligned} \epsilon_{0x} &= \frac{\partial u_0}{\partial x} + \frac{1}{2} \left(\frac{\partial w_0}{\partial x} \right)^2 \\ \epsilon_{0\theta} &= \frac{1}{R(x)} \frac{\partial v_0}{\partial \theta} + \frac{u_0 \sin \alpha}{R(x)} + \frac{w_0 \cos \alpha}{R(x)} \\ &+ \frac{1}{2R(x)^2} \left(\frac{\partial w_0}{\partial \theta} \right)^2 \\ \epsilon_{0x\theta} &= \frac{\partial v_0}{\partial x} + \frac{1}{R(x)} \frac{\partial u_0}{\partial \theta} - \frac{v_0 \sin \alpha}{R(x)} \\ &+ \frac{1}{R(x)} \frac{\partial w_0}{\partial x} \frac{\partial w_0}{\partial \theta} \end{aligned} \quad (2)$$

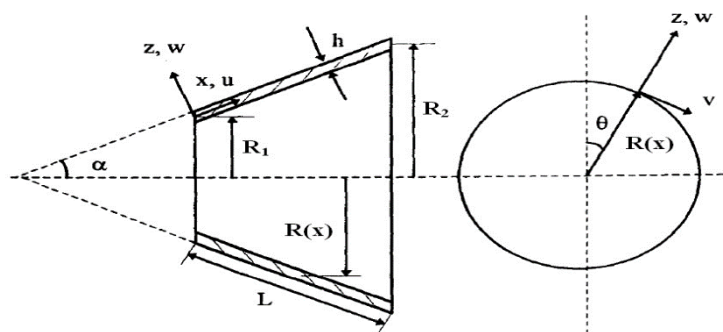


Fig. 1. Image of the schematic of the MEE composite conical shell and coordinate system [60]

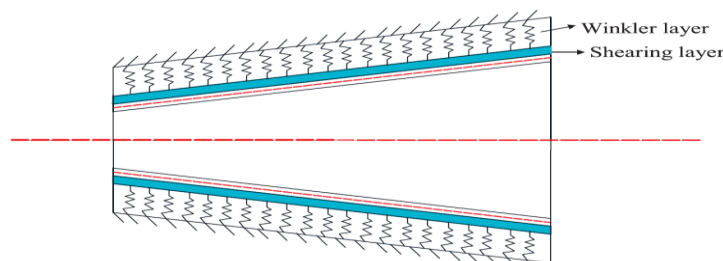


Fig. 2. Image of schematic of the conical shell on the nonlinear elastic foundation [39]

$$k_x = \frac{\partial \psi_x}{\partial x}, \quad k_\theta = \frac{1}{R(x)} \left(\frac{\partial \beta_\theta}{\partial \theta} + \beta_x \sin \alpha \right), \quad (3)$$

$$k_{x\theta} = \frac{\partial \beta_\theta}{\partial x} + \frac{1}{R(x)} \frac{\partial \beta_x}{\partial \theta} - \frac{\beta_\theta \sin \alpha}{R(x)}$$

$$\varepsilon_{xz} = \frac{\partial w_0}{\partial x} + \beta_x, \quad (4)$$

$$\varepsilon_{\theta z} = \frac{1}{R(x)} \frac{\partial w_0}{\partial \theta} - \frac{v_0 \cos \alpha}{R(x)} + \beta_\theta$$

It should be mentioned that u_0 , v_0 and w_0 denote the displacements of an arbitrary point on the middle surface of the conical shell located at point $(x, \theta, 0)$ [61]. In addition, β_x and β_θ refer to the total angular rotations of the line normal to the middle surface about θ and x axes, respectively [61].

2.2. Stress-strain Relations

The coupled constitutive relations for the MEE shell can be expressed as following [63, 64 quoted from 65-68]:

$$\begin{Bmatrix} \sigma_x \\ \sigma_\theta \\ \sigma_{\theta z} \\ \sigma_{xz} \\ \sigma_{x\theta} \end{Bmatrix} = \begin{bmatrix} c_{11} & c_{12} & 0 & 0 & 0 \\ c_{12} & c_{22} & 0 & 0 & 0 \\ 0 & 0 & c_{44} & 0 & 0 \\ 0 & 0 & 0 & c_{44} & 0 \\ 0 & 0 & 0 & 0 & c_{66} \end{bmatrix} \begin{Bmatrix} \varepsilon_x \\ \varepsilon_\theta \\ \varepsilon_{\theta z} \\ \varepsilon_{xz} \\ \varepsilon_{x\theta} \end{Bmatrix} - \begin{bmatrix} 0 & 0 & e_{31} \\ 0 & 0 & e_{31} \\ 0 & e_{24} & 0 \\ e_{15} & 0 & 0 \\ 0 & 0 & 0 \end{bmatrix} \begin{Bmatrix} E_x \\ E_\theta \\ E_z \end{Bmatrix} - \begin{bmatrix} 0 & 0 & s_{31} \\ 0 & 0 & s_{31} \\ 0 & s_{24} & 0 \\ s_{15} & 0 & 0 \\ 0 & 0 & 0 \end{bmatrix} \begin{Bmatrix} H_x \\ H_\theta \\ H_z \end{Bmatrix} \quad (5)$$

$$\begin{Bmatrix} D_x \\ D_\theta \\ D_z \end{Bmatrix} = \begin{bmatrix} 0 & 0 & 0 & e_{15} & 0 \\ 0 & 0 & e_{24} & 0 & 0 \\ e_{31} & e_{31} & 0 & 0 & 0 \end{bmatrix} \begin{Bmatrix} \varepsilon_x \\ \varepsilon_\theta \\ \varepsilon_{\theta z} \\ \varepsilon_{xz} \\ \varepsilon_{x\theta} \end{Bmatrix} + \begin{bmatrix} h_{11} & 0 & 0 \\ 0 & h_{22} & 0 \\ 0 & 0 & h_{33} \end{bmatrix} \begin{Bmatrix} E_x \\ E_\theta \\ E_z \end{Bmatrix} + \begin{bmatrix} g_{11} & 0 & 0 \\ 0 & g_{22} & 0 \\ 0 & 0 & g_{33} \end{bmatrix} \begin{Bmatrix} H_x \\ H_\theta \\ H_z \end{Bmatrix} \quad (6)$$

$$\begin{Bmatrix} B_x \\ B_\theta \\ B_z \end{Bmatrix} = \begin{bmatrix} 0 & 0 & 0 & s_{15} & 0 \\ 0 & 0 & s_{24} & 0 & 0 \\ s_{31} & s_{31} & 0 & 0 & 0 \end{bmatrix} \begin{Bmatrix} \varepsilon_x \\ \varepsilon_\theta \\ \varepsilon_{\theta z} \\ \varepsilon_{xz} \\ \varepsilon_{x\theta} \end{Bmatrix} + \begin{bmatrix} g_{11} & 0 & 0 \\ 0 & g_{22} & 0 \\ 0 & 0 & g_{33} \end{bmatrix} \begin{Bmatrix} E_x \\ E_\theta \\ E_z \end{Bmatrix} + \begin{bmatrix} \mu_{11} & 0 & 0 \\ 0 & \mu_{22} & 0 \\ 0 & 0 & \mu_{33} \end{bmatrix} \begin{Bmatrix} H_x \\ H_\theta \\ H_z \end{Bmatrix} \quad (7)$$

while $\{\sigma_x, \sigma_\theta, \sigma_{\theta z}, \sigma_{xz}, \sigma_{x\theta}\}^T$, $\{\varepsilon_x, \varepsilon_\theta, \varepsilon_{\theta z}, \varepsilon_{xz}, \varepsilon_{x\theta}\}^T$, $\mathbf{E} = \{E_x, E_\theta, E_z\}^T$ and $\mathbf{H} = \{H_x, H_\theta, H_z\}^T$ refer to stress, strain, electric field, and magnetic field vectors, respectively [64]. Besides, $\{D_x, D_\theta, D_z\}^T$ and $\{B_x, B_\theta, B_z\}^T$ denote electric displacement and magnetic induction vectors, respectively [63-64]. In addition, $[c_{ij}]$, $[e_{ij}]$ and $[s_{ij}]$ imply matrices of elastic, piezoelectric, and piezomagnetic coefficients, respectively [63-64]. It should be mentioned that $[h_{ij}]$, $[g_{ij}]$ and $[\mu_{ij}]$ are respectively the matrices of dielectric, magnetoelectric, and magnetic permeability coefficients [64].

If the electric vector and magnetic intensity are respectively written as gradients of the scalar electric (ϕ) and magnetic (ψ) potentials, vector equations of Maxwell in the quasi-static approximation are satisfied [63]:

$$\mathbf{E} = -\nabla \phi, \quad \mathbf{H} = -\nabla \psi \quad (8)$$

In this paper, because of the thin nature of the shell, the components of in-plane electric and magnetic fields are ignored ($E_x = 0, E_\theta = 0, H_x = 0, H_\theta = 0$) [69 quoted from 70].

Equations (9) and (10) show Gauss' laws for electrostatics and magnetostatics which can be used to obtain the electromagnetic state of the shell [17 quoted from 71]:

$$D_{x,x} + \frac{1}{R(x)} D_{\theta,\theta} + D_{z,z} = 0 \quad (9)$$

$$B_{x,x} + \frac{1}{R(x)} B_{\theta,\theta} + B_{z,z} = 0 \quad (10)$$

Considering magneto-electric boundary conditions ($\phi(-0.5h) = 0$, $\phi(0.5h) = V_0$, $\psi(-0.5h) = 0$, $\psi(0.5h) = \Omega_0$) [17] and the previous assumptions that $\phi_{,x} = 0$, $\phi_{,\theta} = 0$,

$\psi_{,x} = 0$ and $\psi_{,\theta} = 0$ lead to the following relations for E_z and H_z :

$$E_z = -\frac{V_0}{h}, \quad H_z = -\frac{\Omega_0}{h} \quad (11)$$

while V_0 and Ω_0 refer to electric and magnetic potentials, respectively [17].

3. Lagrange Method

In order to extract the nonlinear ordinary differential equation of the system, for the considered problem, the Lagrange method equation [61] can be used:

$$\frac{\partial L}{\partial q_i} - \frac{d}{dt} \left(\frac{\partial L}{\partial \dot{q}_i} \right) = 0, i = 1, \dots, 5, \quad (12)$$

$$q_1 = u_0, q_2 = w_0, q_3 = w_0, q_4 = \beta_x, q_5 = \beta_\theta$$

Whereas $L = T - U_\varepsilon - U_k$. It should be mentioned that T and U_ε refer to kinetic and strain energies [61] while U_k denotes energy due to a nonlinear foundation. Required relations of these energies can be obtained through equations (13) to (15):

$$U_\varepsilon = \frac{1}{2} \int_x \int_\theta \int_z \begin{pmatrix} \sigma_x \varepsilon_x + \sigma_\theta \varepsilon_\theta \\ + \sigma_{x\theta} \varepsilon_{x\theta} + \sigma_{xz} \varepsilon_{xz} \\ + \sigma_{\theta z} \varepsilon_{\theta z} \end{pmatrix} R(x) dz d\theta dx \quad (13)$$

$$T = \frac{1}{2} \int_x \int_\theta \begin{pmatrix} I_1 (\dot{u}_0^2 + \dot{v}_0^2 + \dot{w}_0^2) \\ + 2I_2 (\dot{u}_0 \dot{\beta}_x + \dot{v}_0 \dot{\beta}_\theta) \\ + I_3 (\dot{\beta}_x^2 + \dot{\beta}_\theta^2) \end{pmatrix} R(x) d\theta dx \quad (14)$$

$$\frac{\partial U_k}{\partial u_0} = 0, \frac{\partial U_k}{\partial v_0} = 0, \frac{\partial U_k}{\partial \psi_x} = 0, \frac{\partial U_k}{\partial \psi_\theta} = 0$$

$$\frac{\partial U_k}{\partial w_0} = \int_x \int_\theta \begin{pmatrix} K_{Lw} w_0 + K_{NLw} w_0^3 \\ - K_p \left(\frac{\partial^2 w_0}{\partial x^2} \right) \\ + \frac{\sin \alpha}{R(x)} \frac{\partial w_0}{\partial x} \\ + \frac{1}{R(x)^2} \frac{\partial^2 w_0}{\partial \theta^2} \end{pmatrix} R(x) d\theta dx \quad (15)$$

$$\frac{\partial U_k}{\partial \dot{u}_0} = 0, \frac{\partial U_k}{\partial \dot{v}_0} = 0, \frac{\partial U_k}{\partial \dot{w}_0} = 0, \frac{\partial U_k}{\partial \dot{\psi}_x} = 0$$

$$, \frac{\partial U_k}{\partial \dot{\psi}_\theta} = 0$$

It is valuable to emphasize that equations (13) and (14) are written based on reference [61] while equation (15) is derived on the basis of references [37, 51]. In equation (14), I_1, I_2 and I_3 denote mass moments of inertia terms [62]. It

should be noted that in equation (15), K_{Lw} and K_{NLw} demonstrate linear and nonlinear constants of the Winkler elastic foundation while K_p indicates the shear stiffness constant of the elastic foundation [51]. In order to derive the nonlinear ordinary differential equation of the vibration, the following relations which satisfy geometrical boundary conditions of the simply supported conical shells $v_0(x, \theta, z) = 0, w_0(x, \theta, z) = 0, \psi_\theta(x, \theta, z) = 0, x = 0, L$ [61, 72] can be used:

$$\begin{cases} u_0(x, \theta, t) = u_t(t) \cos \frac{m\pi x}{L} \cos n\theta \\ v_0(x, \theta, t) = v_t(t) \sin \frac{m\pi x}{L} \sin n\theta \\ w_0(x, \theta, t) = w_t(t) \sin \frac{m\pi x}{L} \cos n\theta \\ \beta_x(x, \theta, t) = \beta_{xt}(t) \cos \frac{m\pi x}{L} \cos n\theta \\ \beta_\theta(x, \theta, t) = \beta_{\theta t}(t) \sin \frac{m\pi x}{L} \sin n\theta \end{cases} \quad (16)$$

The displacement and rotation relations of equation (16) are written based on the reference [61] while m and n demonstrate half-wave numbers of displacements in the length and circumference of the shell, respectively [61], and (m, n) refers to the vibration mode shape. Substituting equation (16) into equations (13) to (15) and then using equation (12) lead to extraction of the nonlinear ordinary differential equation of the system:

$$\mathbf{M}\ddot{\mathbf{x}} + \mathbf{K}\mathbf{x} + \mathbf{b}w_t^3 = \mathbf{0}, \quad (17)$$

$$\mathbf{x} = \{u_t, v_t, w_t, \beta_{xt}, \beta_{\theta t}\}^T$$

while \mathbf{M} and \mathbf{K} respectively demonstrate mass and stiffness matrices and \mathbf{b} is the vector of nonlinear coefficients caused by geometric nonlinearity and nonlinearity of elastic foundation.

4. Lindstedt-Poincare Method and Modal Analysis

In order to use the Lindstedt-Poincare method, a new independent variable $\tau = \omega_{NL} t$ is defined [73]; thus the relation $\ddot{\mathbf{x}} = d^2 \mathbf{x} / dt^2 = \omega^2 d^2 \mathbf{x} / d\tau^2$ is acquired. In addition, the variables ω_{NL}, \mathbf{x} and w_t should be considered as following [73]:

$$\omega_{NL}(\varepsilon) = \omega_0 + \varepsilon \omega_1 + \varepsilon^2 \omega_2 \quad (18)$$

$$\mathbf{x}(t; \varepsilon) = \varepsilon \mathbf{x}_1(\tau) + \varepsilon^2 \mathbf{x}_2(\tau) + \varepsilon^3 \mathbf{x}_3(\tau), \quad (19)$$

$$w_t(t; \varepsilon) = \varepsilon w_1(\tau) + \varepsilon^2 w_2(\tau) + \varepsilon^3 w_3(\tau)$$

while ω_0 denotes the fundamental linear frequency ($\omega_0 = \omega_L$) of the conical shell. Using mentioned relations, one can rewrite equation (17) as shown in equation (20):

$$(\omega_0 + \varepsilon\omega_1 + \varepsilon^2\omega_2)^2 \mathbf{M} \frac{d^2(\varepsilon\mathbf{x}_1 + \varepsilon^2\mathbf{x}_2 + \varepsilon^3\mathbf{x}_3)}{d\tau^2} + \mathbf{K}(\varepsilon\mathbf{x}_1 + \varepsilon^2\mathbf{x}_2 + \varepsilon^3\mathbf{x}_3) + \mathbf{b}(\varepsilon w_1 + \varepsilon^2 w_2 + \varepsilon^3 w_3)^3 = \mathbf{0} \quad (20)$$

By performing some mathematical operations and setting the coefficients of ε , ε^2 and ε^3 equal to zero, equations (21) to (23) are acquired which are respectively coefficients of ε , ε^2 and ε^3 :

$$(\varepsilon) \Rightarrow \omega_0^2 \mathbf{M} \frac{d^2 \mathbf{x}_1}{d\tau^2} + \mathbf{K} \mathbf{x}_1 = \mathbf{0} \quad (21)$$

$$(\varepsilon^2) \Rightarrow 2\omega_1\omega_0 \mathbf{M} \frac{d^2 \mathbf{x}_1}{d\tau^2} + \omega_0^2 \mathbf{M} \frac{d^2 \mathbf{x}_2}{d\tau^2} + \mathbf{K} \mathbf{x}_2 = \mathbf{0} \quad (22)$$

$$(\varepsilon^3) \Rightarrow (2\omega_2\omega_0 + \omega_1^2) \mathbf{M} \frac{d^2 \mathbf{x}_1}{d\tau^2} + 2\omega_1\omega_0 \mathbf{M} \frac{d^2 \mathbf{x}_2}{d\tau^2} + \omega_0^2 \mathbf{M} \frac{d^2 \mathbf{x}_3}{d\tau^2} + \mathbf{K} \mathbf{x}_3 + \mathbf{b} w_1^3 = \mathbf{0} \quad (23)$$

In order to obtain the response of equation (21), applying modal analysis relation $\mathbf{x}_1 = \mathbf{X}\{\zeta_1\}$ [61] results in equation (24). It is important to mention that \mathbf{X} and $\{\zeta_1\}$ denote modal matrix and modal coordinates vector, respectively [61].

$$\omega_0^2 \frac{d^2 \{\zeta_1\}}{d\tau^2} + [\omega_i^2] \{\zeta_1\} = \mathbf{0} \Rightarrow [\omega_i^2] = \mathbf{X}^{-1} \mathbf{M}^{-1} \mathbf{K} \mathbf{X} \quad (24)$$

The row of equation (24) which includes ω_0^2 term of matrix $[\omega_i^2]$ and its response is as following:

$$\varepsilon \Rightarrow \frac{d^2 \zeta_{1s}}{d\tau^2} + \zeta_{1s} = 0 \Rightarrow \zeta_{1s} = \tilde{A} \cos(\tau + \gamma) \quad (25)$$

Substituting modal analysis relations $\mathbf{x}_1 = \mathbf{X}\{\zeta_1\}$ and $\mathbf{x}_2 = \mathbf{X}\{\zeta_2\}$ [61] into equation (22) leads to the acquisition of equation (26):

$$\omega_0^2 \frac{d^2 \{\zeta_2\}}{d\tau^2} + [\omega_i^2] \{\zeta_2\} = -2\omega_1\omega_0 \frac{d^2 \{\zeta_1\}}{d\tau^2} \quad (26)$$

Substituting equation (25) into the row of equation (26) which contains ω_0^2 component of the matrix $[\omega_i^2]$ eventuates to $\omega_1 = 0$ and particular solution of $\zeta_{2s} = 0$. Putting modal analysis relations $\mathbf{x}_1 = \mathbf{X}\{\zeta_1\}$, $\mathbf{x}_2 = \mathbf{X}\{\zeta_2\}$ and $\mathbf{x}_3 = \mathbf{X}\{\zeta_3\}$ [61] into equation (23) and doing

some simplifications lead to the obtaining of equation (27):

$$\omega_0^2 \frac{d^2 \{\zeta_3\}}{d\tau^2} + [\omega_i^2] \{\zeta_3\} = - (2\omega_2\omega_0 + \omega_1^2) \frac{d^2 \{\zeta_1\}}{d\tau^2} - 2\omega_1\omega_0 \frac{d^2 \{\zeta_2\}}{d\tau^2} - \tilde{\mathbf{b}} w_1^3 \quad (27)$$

Neglecting the terms that contain other frequencies than ω_0 from the row of equation (27) which contains ω_0^2 term of matrix $[\omega_i^2]$ and utilizing equation (25) and also $\omega_1 = 0$ and $\zeta_{2s} = 0$ lead to the following equation:

$$\frac{d^2 \zeta_{3s}}{d\tau^2} + \zeta_{3s} = \left(\frac{2\omega_2}{\omega_0} \tilde{A} - \frac{3\tilde{b}_s \tilde{A}^3 (\mathbf{X}(3,s))}{4\omega_0^2} \right) \cos(\tau + \gamma) - \frac{\tilde{b}_s \tilde{A}^3 (\mathbf{X}(3,s))^3}{4\omega_0^2} \cos 3(\tau + \gamma) \quad (28)$$

In order to derive a finite response for equation (28), it is necessary to put the coefficient of $\cos(\tau + \gamma)$ equal to zero

($(2\omega_2/\omega_0) \tilde{A} - (3\tilde{b}_s \tilde{A}^3 (\mathbf{X}(3,s))^3 / 4\omega_0^2) = 0$) which leads to $\omega_2 = 3\tilde{b}_s \tilde{A}^2 (\mathbf{X}(3,s))^3 / 8\omega_0$ and also a particular solution of $\zeta_{3s} = (\tilde{b}_s \tilde{A}^3 (\mathbf{X}(3,s))^3 / 32\omega_0^2) \cos 3(\tau + \gamma)$. Finally, the term of w_t which is only related to fundamental linear frequency ($w_{t\omega_L}$) can be obtained as:

$$w_{t\omega_L} = A \cos(\omega_{NL} t + \gamma), \quad A = \varepsilon \mathbf{X}(3,s) \tilde{A} \quad (29)$$

In addition, putting the results obtained for ω_0 , ω_1 and ω_2 into equation (18) leads to obtain of the following relation for nonlinear frequency ratio (ω_{NL} / ω_L):

$$\frac{\omega_{NL}}{\omega_0} = 1 + \frac{gA^2}{\omega_0^2}, \quad g = \frac{3\tilde{b}_s \mathbf{X}(3,s)}{8} \quad (30)$$

Equation (30) indicates that the nonlinear frequency ratio has a direct relation with nonlinear parameter g . Furthermore, ω_{NL} / ω_L has a direct relation with the square of the amplitude parameter (A^2) while its relation with the square of the fundamental linear frequency is inverse.

5. Results and Discussions

The purpose of this paper is the investigation of the nonlinear vibration of MEE composite

conical shells on a nonlinear elastic foundation under electric or magnetic potential. In order to validate this study, Table 1 compares the frequency parameter ($\omega^* = \omega_0 R_2 \sqrt{(1-\nu^2)/E}$) results of this study with literature (references [74] and [75]) for an isotropic simply supported conical shell with constants of $L \sin \alpha / R_2 = 0.25$ and $h/R_2 = 0.01$ while E and ν denote Young modulus and Poisson ratio, respectively. According to this table, one can conclude that in most cases there is good agreement between the results of this study and the literature.

Table 2 shows the frequency results (Hz) obtained for an isotropic cylindrical shell on a linear elastic foundation with constants of $E = 210 \text{ GPa}$, $\rho = 7850 \text{ kg/m}^3$, $\nu = 0.3$, $L = 0.41 \text{ m}$, $R = 0.3015 \text{ m}$, $h = 1 \text{ mm}$ and $m = 1$ and compares the results with the results of reference [76]. It is noteworthy to mention that R and ρ refer to the radius of the cylindrical shell on the middle surface and the mass density, respectively. The results of Table 2 are for different values of the constants of the foundation and half-wave number of displacement in the circumference of the shell (n). This table demonstrates very good agreement between the results of this paper and the reference [76] which could be evidence for the validity of the present research.

After validation studies, it is time to investigate the vibration responses of the MEE conical shell on a nonlinear elastic foundation. It is important to mention that BaTiO₃-CoFe₂O₄ composite material is chosen as MEE material.

The constants used in this study are extracted based on the constants introduced in reference [64] for piezoelectric BaTiO₃ material and magnetostrictive CoFe₂O₄ material unless the values of the densities of the materials.

The values of densities are $\rho = 5300 \text{ kg/m}^3$ for CoFe₂O₄ and $\rho = 5800 \text{ kg/m}^3$ for BaTiO₃ [77]. Because of the importance of obtaining of the constants of BaTiO₃-CoFe₂O₄ composite material, some explanations are required. References [64] and [77] are provided the constants of BaTiO₃ and CoFe₂O₄ materials, separately. In order to obtain the constants of BaTiO₃-CoFe₂O₄ composite material, in this paper, the average of the constants of BaTiO₃ and CoFe₂O₄ materials is used. The constants of reference [64] are for a situation that normal strain (ϵ_z) and normal stress (σ_z) are considered. In the present paper, $\epsilon_z = 0$ and $\sigma_z = 0$; so it is necessary to do some operations which are based on reference [62].

The equation of MEE material can be written as $\{\sigma_i\} = [c_{ik}]\{\epsilon_k\} - [e_{ij}]\{E_j\} - [s_{ij}]\{H_j\}$ [64 quoted from 65-68] which can be easily converted to $\{\epsilon_k\} = [c_{ik}]^{-1}\{\sigma_i\} + [c_{ik}]^{-1}[e_{ij}]\{E_j\} + [c_{ik}]^{-1}[s_{ij}]\{H_j\}$. Therefore, it is necessary to obtain matrices $[c_{ik}]^{-1}$, $[c_{ik}]^{-1}[e_{ij}]$ as well as $[c_{ik}]^{-1}[s_{ij}]$ and eliminate rows and columns that correspond to σ_z and ϵ_z . Doing this simple operation leads to obtain of the constants of the MEE composite material as shown in Table 3:

Table 1. Comparison of frequency parameter results of this study and literature for isotropic conical shells with different semi-vertex angle values

n	$\alpha = 30^\circ$			$\alpha = 45^\circ$		
	Present	Reference [74]	Reference [75]	Present	Reference [74]	Reference [75]
2	0.8416	0.7910	0.8431	0.7656	0.6879	0.7642
3	0.7415	0.7284	0.7416	0.7253	0.6973	0.7211
4	0.6468	0.6352	0.6419	0.6838	0.6664	0.6747
5	0.5730	0.5531	0.5590	0.6500	0.6304	0.6336
6	0.5278	0.4949	0.5008	0.6306	0.6032	0.6049

Table 2. Comparison of the frequencies (Hz) of the present study with literature for isotropic cylindrical shells surrounded by elastic foundation

n	$K_{Lw} = 2.5 \times 10^7 \text{ N/m}^3$ $K_p = 0 \text{ N/m}$		$K_{Lw} = 0 \text{ N/m}^3$ $K_p = 2.5 \times 10^7 \text{ N/m}$	
	Present	Reference [76]	Present	Reference [76]
3	1004.3852	1004.4	3481.5571	3481.6
5	551.6140	551.57	5072.7267	5072.8
7	412.4312	412.38	6858.0504	6858.2
9	402.0576	402.02	8689.5038	8689.8
11	458.2785	458.29	10540.4502	10541.0
13	557.8284	557.93	12402.5127	12403.5

Table 3. The values of the constants of the composite MEE material

c_{11}	$1.544446697566628 \times 10^{11}$ N/m ²
c_{22}	$1.544446697566628 \times 10^{11}$ N/m ²
c_{12}	$5.34446697566628 \times 10^{10}$ N/m ²
c_{44}	4.415×10^{10} N/m ²
c_{66}	5.05×10^{10} N/m ²
e_{31}	-7.5558516801854 C/m ²
e_{24}	5.8 C/m ²
e_{15}	5.8 C/m ²
s_{31}	88.672074159907282 N/(A.m)
s_{24}	275 N/(A.m)
s_{15}	275 N/(A.m)

In addition, the average of the densities is derived as $\rho = 5550$ kg/m³.

It is necessary to mention that the results of this study are acquired for MEE composite conical shell with $L = 0.6$ m, $\alpha = 15^\circ$, $R_2 = 1$ m and $h = 5$ mm on nonlinear elastic foundation with constants $K_{NLw} = 3 \times 10^{10}$ N/m⁵, $K_{Lw} = 1.8 \times 10^7$ N/m³ and $K_p = 1.8 \times 10^7$ N/m. All constants used in this paper are as mentioned unless other values are emphasized. In addition, all results for MEE composite conical shell are acquired for the mode shape $(m, n) = (1, 3)$.

Table 4 presents the values of fundamental linear frequency as well as nonlinear parameter (g) for different values of the constants of the elastic foundation for shells subjected to electric or magnetic potential.

This table indicates that the value of fundamental linear frequency doesn't have any

change with the change of the value of K_{NLw} . This is because of the fact that K_{NLw} is a nonlinear parameter; so it has no effect on the fundamental linear frequency. On the other hand, according to this table, one can conclude that as one of the linear constants (K_{Lw} or K_p) of the elastic foundation increases, the fundamental linear frequency gets higher values; because the increase of K_{Lw} or K_p increases the linear stiffness of the system which leads to greater fundamental linear frequency. Also, Table 4 indicates that g increases with an increase of K_{NLw} while an increase of the linear constants of the elastic foundation (K_{Lw} or K_p) causes a decrease of g . This is because of the fact that K_{NLw} is a nonlinear parameter and its increase leads to the increase of the nonlinearity of the system which appears in g . On the other hand, when K_{Lw} or K_p , which are linear parameters, increases, the rate of the nonlinearity of the system decreases which leads to the decrease of g .

Figures 3 (a) and (b) depict the effect of the nonlinear constant of the elastic foundation on the curves of nonlinear frequency ratio versus amplitude parameter in the presence of electric and magnetic potentials, respectively. These figures illustrate that in the presence of electric or magnetic potential, the increase of the nonlinear constant of the elastic foundation causes the increase of the nonlinear frequency ratio. This is because of the fact that as shown in Table 4, the increase of K_{NLw} leads to the increase of the nonlinear parameter (g) which according to equation (30) causes a greater nonlinear frequency ratio.

Table 4. The influence of the constants of the elastic foundation on the vibration characteristics of the considered MEE composite conical shell

Constants of elastic foundation		$V_0 = 9 \times 10^4$ V, $\Omega_0 = 0$ A		$V_0 = 0$ V, $\Omega_0 = 9 \times 10^4$ A	
		ω_L (rad/s)	g (m ⁻² s ⁻²)	ω_L (rad/s)	g (m ⁻² s ⁻²)
$K_{Lw} = 1.8 \times 10^7$ N/m ³ ,	$K_{NLw} = 0$ N/m ⁵	6139.36	$2.62566377386 \times 10^9$	6588.06	$2.62262611940 \times 10^9$
	$K_{NLw} = 3 \times 10^{10}$ N/m ⁵	6139.36	$2.84538340985 \times 10^9$	6588.06	$2.84209155973 \times 10^9$
$K_p = 1.8 \times 10^7$ N/m	$K_{NLw} = 6 \times 10^{10}$ N/m ⁵	6139.36	$3.06510304584 \times 10^9$	6588.06	$3.06155700006 \times 10^9$
	$K_{NLw} = 9 \times 10^{10}$ N/m ⁵	6139.36	$3.28482268183 \times 10^9$	6588.06	$3.28102244040 \times 10^9$
$K_{NLw} = 3 \times 10^{10}$ N/m ⁵ ,	$K_{Lw} = 0$ N/m ³	6088.25	$2.84573378179 \times 10^9$	6540.51	$2.84245955485 \times 10^9$
	$K_{Lw} = 0.9 \times 10^7$ N/m ³	6113.86	$2.84555882891 \times 10^9$	6564.33	$2.84227580630 \times 10^9$
$K_p = 1.8 \times 10^7$ N/m	$K_{Lw} = 1.8 \times 10^7$ N/m ³	6139.36	$2.84538340985 \times 10^9$	6588.06	$2.84209155973 \times 10^9$
	$K_{Lw} = 2.7 \times 10^7$ N/m ³	6164.76	$2.84520752293 \times 10^9$	6611.70	$2.84190681331 \times 10^9$
$K_{Lw} = 1.8 \times 10^7$ N/m ³ ,	$K_p = 0$ N/m	3726.60	$2.85749650580 \times 10^9$	4429.81	$2.85479386461 \times 10^9$
	$K_p = 0.9 \times 10^7$ N/m	5079.60	$2.85173587305 \times 10^9$	5614.81	$2.84875824664 \times 10^9$
$K_{NLw} = 3 \times 10^{10}$ N/m ⁵	$K_p = 1.8 \times 10^7$ N/m	6139.36	$2.84538340985 \times 10^9$	6588.06	$2.84209155973 \times 10^9$
	$K_p = 2.7 \times 10^7$ N/m	7039.42	$2.83835391924 \times 10^9$	7433.01	$2.83470151164 \times 10^9$

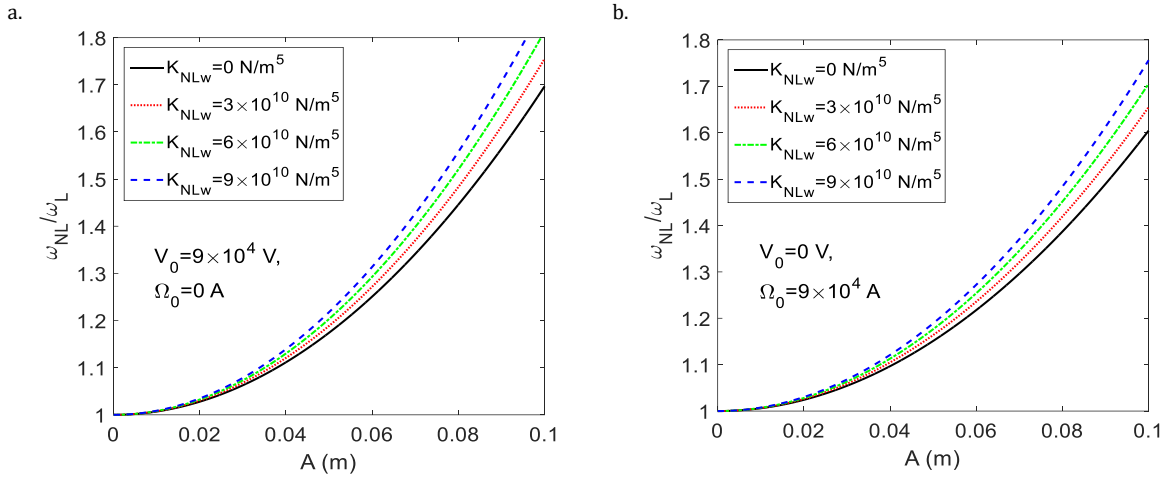


Figure 3. The influence of the nonlinear constant of the foundation on the $\omega_{NL}/\omega_L - A$ diagrams in the presence of, a: electric potential, b: magnetic potential

Figures 4 (a) and (b) show diagrams of nonlinear frequency ratio versus amplitude parameters for different values of K_{Lw} in the presence of electric and magnetic potentials, respectively. These figures demonstrate that the change of K_{Lw} has a low impact on the nonlinear frequency ratio versus amplitude parameter diagrams. However, more precision in Figures 4 (a) and (b) reveals that, for the constant amplitude parameter, the increase of K_{Lw} leads to the decrease of the nonlinear frequency ratio. This is due to the reason that the increase of K_{Lw} leads to greater linear stiffness of the system and so as depicted in Table 4, greater fundamental linear frequency.

In addition, according to Table 4, g gets smaller values with an increase of K_{Lw} . As shown in equation (30), the mentioned facts lead to the decrease of the nonlinear frequency ratio of the considered MEE composite conical shell.

Figures 5 (a) and (b) display diagrams of nonlinear frequency ratio against amplitude parameters in the presence of electric and magnetic potentials, respectively, while K_p getting different values. Looking at these figures leads to the conclusion that for a constant value of A , the increase of K_p leads to a decrease in the value of the nonlinear frequency ratio.

This conclusion can be explained as following: As shown in Table 4, the increase of K_p causes smaller values for g and greater values for fundamental linear frequency. It is apparent from equation (30) that the decrease of g and the increase of ω_L result in a smaller nonlinear frequency ratio.

In addition to the noted results, Figures 3 to 5 indicate that the greater the amplitude parameter, the greater the nonlinear frequency ratio; because the increase of the amplitude parameter as shown in equation (30), makes the nonlinear effects more apparent.

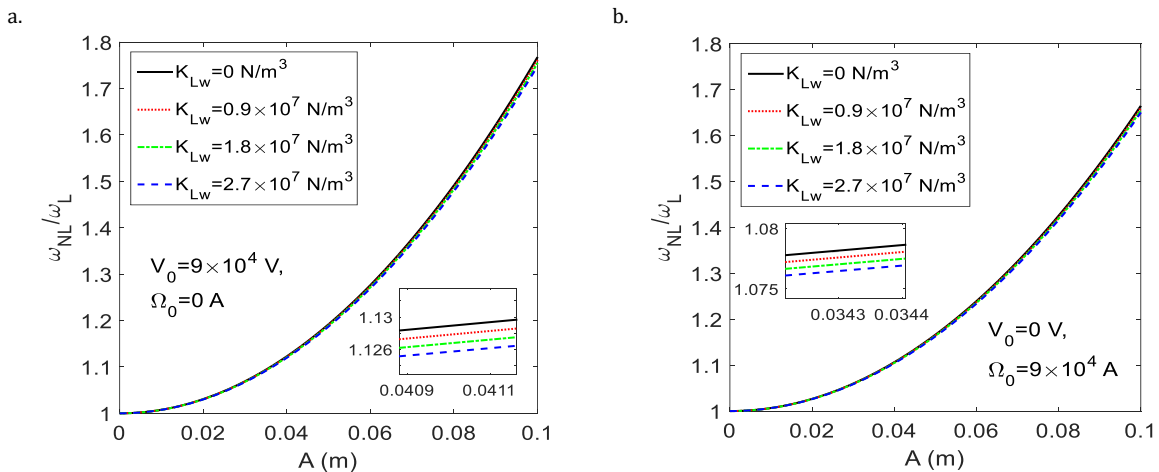


Figure 4. Diagrams of $\omega_{NL}/\omega_L - A$ for different values of the foundation constant K_{Lw} when, a: V_0 , b: Ω_0 , exists

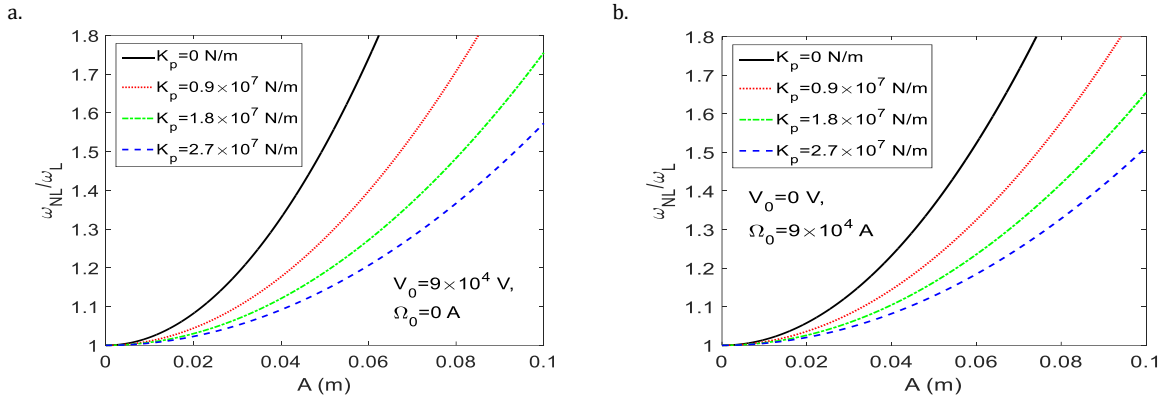


Figure 5. The curves of nonlinear frequency ratio against amplitude parameter for different values of K_p in the condition that, a: $V_0 = 9 \times 10^4$ V, $\Omega_0 = 0$ A , b: $\Omega_0 = 9 \times 10^4$ A, $V_0 = 0$ V

Figure 6 represents a diagram of the nonlinear frequency ratio versus the electric potential for different values of amplitude parameter while $\Omega_0 = 0$ A . It may be helpful to mention that $V_0 = [-90000, -9000, -900, -90, -9, 0, 9, 90, 900, 9000, 90000]$ V. Figure 6 shows that as the electric potential moves from -90000 to 90000, the nonlinear frequency ratio gets higher values. The reason for this behavior can be explained as follows: the movement of electric potential from negative values to positive ones leads to a decrease of the linear part of stress which strengthens the nonlinearity of the system; this is apparent from equations (5) and (11) as well as Table 3. Besides, in order to illustrate the reason for this behavior, Table 5 could be helpful. Table 5 shows the values of fundamental linear frequency and nonlinear parameters for different values of electric potential while the magnetic potential is considered to be zero. This table indicates that the nonlinear parameter increases and in most cases, the fundamental linear frequency decreases with the movement of electric potential from -90000 V to 90000 V which according to equation (30), justifies the increase of the nonlinear frequency ratio in the considered situations. Another result of Figure 6 is that for a constant value of V_0 , as the value of the amplitude parameter increases, the nonlinear frequency ratio gets higher values.

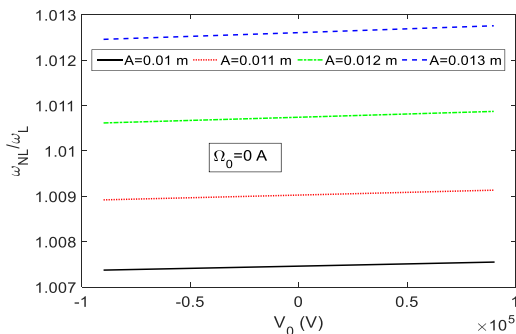


Figure 6. The curves of nonlinear frequency ratio against the electric potential for different amplitude parameter values

Table 5. The impression of the electric potential on the values of fundamental linear frequency and nonlinear parameter (g)

V_0 (V)	$\Omega_0 = 0$ A	
	ω_L (rad/s)	g ($m^{-2}s^{-2}$)
-90000	6212.01	$2.84487707706 \times 10^9$
-9000	6179.42	$2.84510540678 \times 10^9$
-900	6176.16	$2.84512819648 \times 10^9$
-90	6175.83	$2.84513047502 \times 10^9$
-9	6175.80	$2.84513070287 \times 10^9$
0	6175.79	$2.84513072818 \times 10^9$
9	6175.79	$2.84513075350 \times 10^9$
90	6175.76	$2.84513098135 \times 10^9$
900	6175.43	$2.84513325979 \times 10^9$
9000	6172.16	$2.84515603989 \times 10^9$
90000	6139.36	$2.84538340985 \times 10^9$

Figure 7 depicts the curves of nonlinear frequency ratio versus the magnetic potential for various amplitude parameter values while $V_0 = 0$ V and $\Omega_0 = [-90000, -9000, -900, -90, -9, 0, 9, 90, 900, 9000, 90000]$ A.

Figure 7 shows that for constant amplitude parameter, the increase of the magnetic potential from -90000 A to 90000 A results in the decrease of the nonlinear frequency ratio. This is because of the fact that the movement of magnetic potential from -90000 A to 90000 A leads to an increase of the linear part of stress which decreases the effect of nonlinearity; according to equations (5) and (11) and also Table 3, this result is obvious. Furthermore, the reason for this behavior can be illustrated with the help of Table 6 as following: Table 6 demonstrates the values of fundamental linear frequency and nonlinear parameters for different magnetic potential values whereas $V_0 = 0$ V . This table shows that with the movement of the magnetic potential from -90000 A to 90000 A, the fundamental linear frequency gets higher values because of the increase of the linear stiffness while the nonlinear parameter becomes smaller. It is apparent from equation (30) that the mentioned

factors cause a decrease in the nonlinear frequency ratio. In addition, one can conclude from Figure 7 that for the constant value of magnetic potential, the greater the amplitude parameter, the higher the nonlinear frequency ratio.

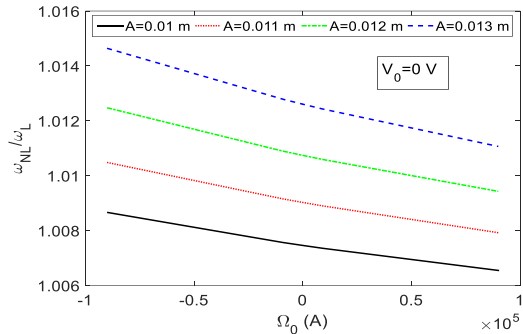


Figure 7. The curves of ω_{NL}/ω_L versus magnetic potential for different values of amplitude parameter

Table 6. The values of vibration characteristics for various values of magnetic potential

Ω_0 (A)	$V_0 = 0$ V	
	ω_L (rad/s)	g ($m^{-2}s^{-2}$)
-90000	5733.48	$2.84803633039 \times 10^9$
-9000	6133.02	$2.84542716565 \times 10^9$
-900	6171.53	$2.84516043188 \times 10^9$
-90	6175.37	$2.84513369915 \times 10^9$
-9	6175.75	$2.84513102528 \times 10^9$
0	6175.79	$2.84513072818 \times 10^9$
9	6175.84	$2.84513043108 \times 10^9$
90	6176.22	$2.84512775708 \times 10^9$
900	6180.05	$2.84510101113 \times 10^9$
9000	6218.27	$2.84483295554 \times 10^9$
90000	6588.06	$2.84209155973 \times 10^9$

Figure 8 (a) demonstrates the curves of nonlinear frequency ratio versus amplitude parameter in the presence of positive electric potential, in the condition without electric and magnetic potentials as well as in the presence of positive magnetic potential. This figure implies that for constant A , the presence of positive magnetic potential leads to the smallest value of the nonlinear frequency ratio. Besides, a comparison of the responses of the system in the presence of positive electric potential and the system without electric and magnetic potentials reveals that for the constant amplitude parameter, the value of the nonlinear frequency ratio is slightly greater for the condition that $V_0 = +9 \times 10^4$ V, $\Omega_0 = 0$ A. The reason for the mentioned results of Figure 8 (a) can be illustrated as follows: in the presence of positive electric potential, the linear part of the stress is smaller in comparison with the situation without electric and magnetic potentials. On the other hand, in the presence of positive magnetic

potential, the linear part of stress is higher in comparison with the situation without electric and magnetic potentials. It should be mentioned that greater linear stress leads to a decrease in the nonlinearity of the system. As can be seen, the effect of the magnetic potential on the diagram is more apparent; this is because of the fact that according to Table 3, the value of s_{31} is much greater than the absolute value of e_{31} . Figure 8 (b) shows the nonlinear frequency ratio against amplitude parameter diagrams for the shells under the negative value of electric potential, without electric and magnetic potentials, and negative value of magnetic potential. It can be concluded from this figure that for a constant value of the amplitude parameter, the value of ω_{NL}/ω_L is the highest in the presence of negative magnetic potential and is the smallest in the presence of negative electric potential. One can explain the reason for the mentioned behaviors of the diagrams of Figure 8 (b) as following: when the system is subjected to negative electric potential, its linear stress is higher than at $\Omega_0 = 0$ A, $V_0 = 0$ V. Conversely, when the system is under negative magnetic potential, its linear stress is smaller in comparison with the system without electric and magnetic potentials. It is apparent that the greater the linear stress, the weaker the effect of the nonlinearity. Because of this fact that the value of s_{31} is much greater than the absolute value of e_{31} , the effect of magnetic potential on the diagram is more apparent. In addition, one can justify the mentioned consequences of Figures 8 (a) and (b) using equation (30) as well as the values of ω_L and g shown in Tables 5 and 6 for conditions considered in Figures 8 (a) and (b).

Table 7 represents the values of vibration characteristics including fundamental linear frequency as well as nonlinear parameters for different thickness values of the MEE composite conical shell. This table demonstrates that as h increases, ω_L acquires smaller values; this is because of this fact that the increase of h leads to an increase in the mass of the shell which leads to a decrease in the fundamental linear frequency. Another outcome of Table 7 is that the value of g decreases as the value of h increases. Figures 9 (a) and (b) show the influence of the thickness of conical shells on the curves of $\omega_{NL}/\omega_L - A$ in the situations with electric and magnetic potentials, respectively. One can figure out from these figures that the value of the nonlinear frequency ratio becomes greater with an increase in the thickness because of the decrease in the fundamental linear frequency as depicted in Table 7.

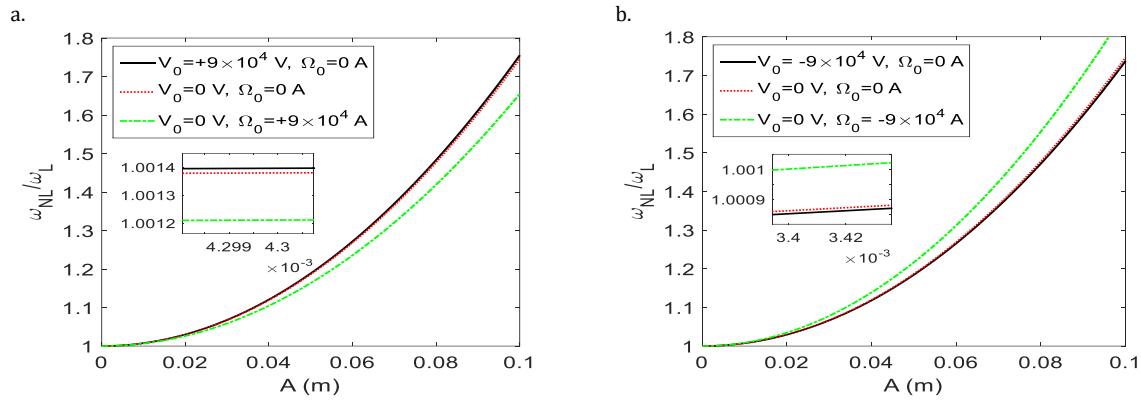


Figure 8. The influence of the electric and magnetic potentials on the nonlinear frequency ratio- amplitude parameter diagrams

Table 7. The values of fundamental linear frequency and nonlinear parameter for MEE composite conical shells with different thickness values

h (mm)	$V_0 = 9 \times 10^4$ V, $\Omega_0 = 0$ A		$V_0 = 0$ V, $\Omega_0 = 9 \times 10^4$ A	
	ω_L (rad/s)	g ($m^{-2}s^{-2}$)	ω_L (rad/s)	g ($m^{-2}s^{-2}$)
3	7319.19	$2.98193856859 \times 10^9$	7940.51	$2.97518489735 \times 10^9$
5	6139.36	$2.84538340985 \times 10^9$	6588.06	$2.84209155973 \times 10^9$
7	5560.87	$2.78600498177 \times 10^9$	5916.77	$2.78384938379 \times 10^9$
9	5216.95	$2.75267178171 \times 10^9$	5513.24	$2.75107293494 \times 10^9$

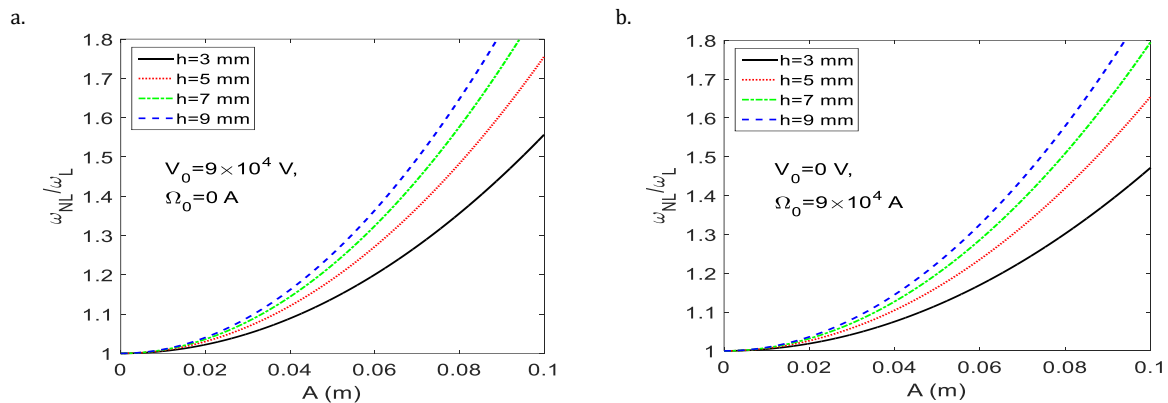


Figure 9. Diagrams of nonlinear frequency ratio versus amplitude parameter for different thickness values for shells under, a: electric potential, b: magnetic potential

Table 8 represents the influence of the length on the fundamental linear frequency and nonlinear parameter (g) of the conical shells under electric or magnetic potential. One can confirm from this table that the increase of the length leads to a decrease in the fundamental linear frequency and g . The reason for the decrease of fundamental linear frequency is the increase of mass due to the increase in length. The effects of the length of the MEE composite conical shell on the nonlinear frequency ratio against amplitude parameter diagrams are

shown in Figures 10 (a) and (b). It is apparent that Figures 10 (a) and (b) are for the shells subjected to electric and magnetic potentials, respectively. One can infer from Figures 10 (a) and (b) that for a determined amplitude parameter, the increase of the length makes smaller values for the nonlinear frequency ratio which is due to the decrease of the nonlinear parameter g as depicted in Table 8.

Another result of Figures 8 to 10 is that the nonlinear frequency ratio becomes higher with an increase in the amplitude parameter.

Table 8. The effect of the length of the MEE composite conical shell on the vibration characteristics

L (m)	$V_0 = 9 \times 10^4$ V, $\Omega_0 = 0$ A		$V_0 = 0$ V, $\Omega_0 = 9 \times 10^4$ A	
	ω_L (rad/s)	g ($m^{-2}s^{-2}$)	ω_L (rad/s)	g ($m^{-2}s^{-2}$)
0.5	6925.35	$5.25805061215 \times 10^9$	7453.19	$5.25426839394 \times 10^9$
0.6	6139.36	$2.84538340985 \times 10^9$	6588.06	$2.84209155973 \times 10^9$
0.7	5540.86	$1.81264427630 \times 10^9$	5940.60	$1.80975483497 \times 10^9$
0.8	5068.12	$1.31636248602 \times 10^9$	5437.30	$1.31377510493 \times 10^9$

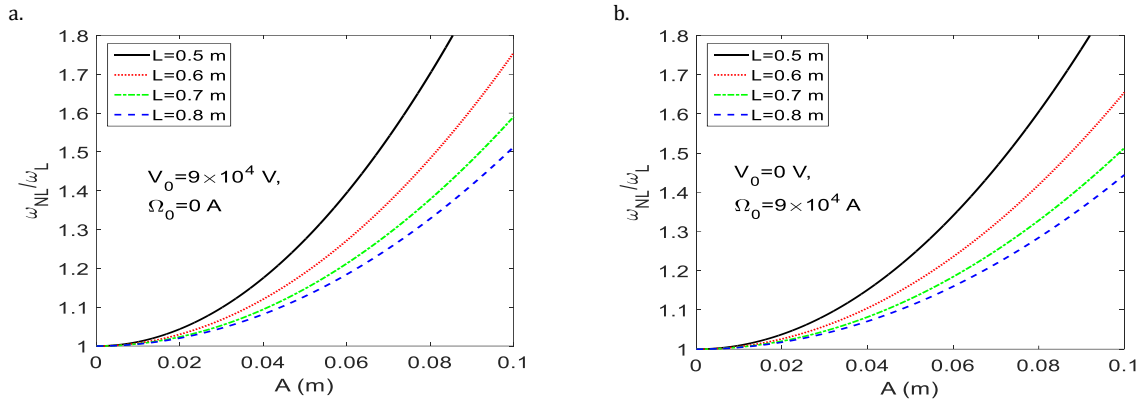


Figure 10. The influence of the length of the MEE composite conical shell on the $\omega_{NL}/\omega_L - A$ curves in the presence of, a: electric potential, b: magnetic potential

6. Conclusions

This paper deals with the nonlinear vibration of an MEE composite conical shell surrounded by a nonlinear elastic foundation subjected to electric or magnetic potential. The relations of strains are extracted considering the effect of shear deformation with the help of the von Karman nonlinear approach. Stress, electric displacement, and magnetic induction vectors are derived using coupled relations of MEE material. Applying quasi-static approximation of Maxwell's vector equations, Gauss' laws for electrostatics and magnetostatics, and considering the thin nature of the MEE composite conical shell lead to the extraction of electric and magnetic fields. The nonlinear ordinary differential equation of the system is extracted via the Lagrange technique while the effect of rotary inertia is considered in the extraction of kinetic energy. Lindstedt-Poincare method and modal analysis are employed to obtain the nonlinear responses of the MEE composite conical shell. The results of the literature are compared with this study's results to investigate the accuracy of the results of this research. The effects of several parameters including the nonlinear and linear constants of elastic foundation, the presence of electric or magnetic potential, thickness and length on the fundamental linear frequency, nonlinear parameter, and the curves of nonlinear frequency

ratio versus amplitude parameter are investigated which can be classified as mentioned below:

1. Fundamental linear frequency does not have any change as the value of the nonlinear constant of the elastic foundation changes.
2. The value of fundamental linear frequency increases with an increase of the linear constants of the elastic foundation or the magnetic field and decreases with an increase in the thickness or the length.
3. Nonlinear parameter gets greater values with an increase of the nonlinear constant of the elastic foundation or the electric potential and decreases with an increase of the linear constants of elastic foundation, magnetic potential, thickness, or length.
4. For constant amplitude parameters, as the value of the nonlinear constant of the elastic foundation or thickness increases, the nonlinear frequency ratio becomes greater.
5. For a determined amplitude parameter, the value of the nonlinear frequency ratio becomes smaller with an increase of the linear constants of elastic foundation or the length.
6. The increase in the amplitude parameter leads to an increase of the nonlinear frequency ratio.

References

- [1] Duc, N. D., Anh, V. T. T. and Cong, P. H., 2014. Nonlinear axisymmetric response of FGM shallow spherical shells on elastic foundations under uniform external pressure and temperature. *European Journal of Mechanics-A/Solids*, 45, pp.80-89.
- [2] Duc, N. D., 2014. Nonlinear static and dynamic stability of functionally graded plates and shells. *Vietnam: Vietnam Natl Univ Press. Google Scholar*.
- [3] Duc, N. D., Cong, P. H., Tuan, N. D., Tran, P. and Van Thanh, N., 2017. Thermal and mechanical stability of functionally graded carbon nanotubes (FG CNT)-reinforced composite truncated conical shells surrounded by the elastic foundations. *Thin-Walled Structures*, 115, pp.300-310.
- [4] Duc, N. D., Seung-Eock, K. and Chan, D. Q., 2018. Thermal buckling analysis of FGM sandwich truncated conical shells reinforced by FGM stiffeners resting on elastic foundations using FSDT. *Journal of Thermal Stresses*, 41(3), pp.331-365.
- [5] Do, Q. C., Pham, D. N., Vu, D. Q., Vu, T. T. A. and Nguyen, D. D., 2019. Nonlinear buckling and post-buckling of functionally graded CNTs reinforced composite truncated conical shells subjected to axial load. *Steel and Composite Structures*, 31.
- [6] Quan, T. Q., Kim, S. E. and Duc, N. D., 2019. Nonlinear dynamic response and vibration of shear deformable piezoelectric functionally graded truncated conical panel in thermal environments. *European Journal of Mechanics-A/Solids*, 77, 103795.
- [7] Chan, D. Q., Long, V. D. and Duc, N. D., 2019. Nonlinear buckling and postbuckling of FGM shear-deformable truncated conical shells reinforced by FGM stiffeners. *Mechanics of Composite Materials*, 54(6), pp.745-764.
- [8] Manh, D. T., Anh, V. T. T., Nguyen, P. D. and Duc, N. D., 2020. Nonlinear post-buckling of CNTs reinforced sandwich-structured composite annular spherical shells. *International Journal of Structural Stability and Dynamics*, 20(02), 2050018.
- [9] Van Thanh, N., Khoa, N. D. and Duc, N. D., 2020. Nonlinear dynamic analysis of piezoelectric functionally graded porous truncated conical panel in thermal environments. *Thin-Walled Structures*, 154, 106837.
- [10] Duc, N. D., Quan, T. Q. and Cong, P. H., 2021. Nonlinear vibration of auxetic plates and shells.
- [11] Zhou, L., Nie, B., Ren, S., Żur, K. K. and Kim, J., 2021. On the hygro-thermo-electro-mechanical coupling effect on static and dynamic responses of piezoelectric beams. *Composite Structures*, 259, 113248.
- [12] Jankowski, P., 2020. Effect of kerr foundation and in-plane forces on free vibration of fgm nanobeams with diverse distribution of porosity. *Acta Mechanica et Automatica*, 14(3), pp.135-143.
- [13] Jankowski, P., Żur, K. K., Kim, J., Lim, C. W. and Reddy, J. N., 2021. On the piezoelectric effect on stability of symmetric FGM porous nanobeams. *Composite Structures*, 267, 113880.
- [14] Żur, K. K., Farajpour, A., Lim, C. W. and Jankowski, P., 2021. On the nonlinear dynamics of porous composite nanobeams connected with fullerenes. *Composite Structures*, 274, 114356.
- [15] Ghobadi, A., Golestanian, H., Beni, Y. T. and Żur, K. K., 2021. On the size-dependent nonlinear thermo-electro-mechanical free vibration analysis of functionally graded flexoelectric nanoplate. *Communications in Nonlinear Science and Numerical Simulation*, 95, 105585.
- [16] Ouakad, H. M. and ŻUR, K. K., 2022. On the snap-through buckling analysis of electrostatic shallow arch micro-actuator via meshless Galerkin decomposition technique. *Engineering Analysis with Boundary Elements*, 134, pp.388-397.
- [17] Razavi, S. and Shoostari, A., 2014. Free vibration analysis of a magneto-electro-elastic doubly-curved shell resting on a Pasternak-type elastic foundation. *Smart Materials and Structures*, 23(10), 105003.
- [18] Bhangale, R. K. and Ganesan, N., 2005. Free vibration studies of simply supported non-homogeneous functionally graded magneto-electro-elastic finite cylindrical shells. *Journal of Sound and Vibration*, 288(1-2), pp.412-422.

- [19] Annigeri, A. R., Ganesan, N. and Swarnamani, S., 2006. Free vibrations of simply supported layered and multiphase magneto-electro-elastic cylindrical shells. *Smart Materials and Structures*, 15(2), 459.
- [20] Tsai, Y. H. and Wu, C. P., 2008. Dynamic responses of functionally graded magneto-electro-elastic shells with open-circuit surface conditions. *International journal of engineering science*, 46(9), pp.843-857.
- [21] Kumaravel, A., Ganesan, N. and Sethuraman, R., 2010. Buckling and vibration analysis of layered and multiphase magneto-electro-elastic cylinders subjected to uniform thermal loading. *Multidiscipline Modeling in Materials and Structures*.
- [22] Lang, Z and Xuewu, L., 2013. Buckling and vibration analysis of functionally graded magneto-electro-thermo-elastic circular cylindrical shells. *Applied Mathematical Modelling*, 37(4), pp.2279-2292.
- [23] Shooshtari, A. and Razavi, S., 2016. Large amplitude free vibration of magneto-electro-elastic curved panels. *Scientia Iranica*, 23(6), pp.2606-2615.
- [24] Shooshtari, A., and Razavi, S., 2015. Linear and nonlinear free vibration of a multilayered magneto-electro-elastic doubly-curved shell on elastic foundation. *Composites Part B: Engineering*, 78, pp. 95-108.
- [25] Mohammadimehr, M., Okhravi, S. V. and Akhavan Alavi, S. M., 2018. Free vibration analysis of magneto-electro-elastic cylindrical composite panel reinforced by various distributions of CNTs with considering open and closed circuits boundary conditions based on FSDT. *Journal of Vibration and Control*, 24(8), pp.1551-1569.
- [26] Vinyas, M and Harursampath, D, 2020. Nonlinear vibrations of magneto-electro-elastic doubly curved shells reinforced with carbon nanotubes. *Composite Structures*, 253, 112749.
- [27] Rostami, R. and Mohammadimehr, M., 2020. Vibration control of rotating sandwich cylindrical shell-reinforced nanocomposite face sheet and porous core integrated with functionally graded magneto-electro-elastic layers. *Engineering with Computers*, pp.1-14.
- [28] Ye, W., Liu, J., Zang, Q. and Lin, G., 2020. Magneto-electro-elastic semi-analytical models for free vibration and transient dynamic responses of composite cylindrical shell structures. *Mechanics of Materials*, 148, 103495.
- [29] Rostami, R., Irani Rahaghi, M. and Mohammadimehr, M., 2021. Vibration control of the rotating sandwich cylindrical shell considering functionally graded core and functionally graded magneto-electro-elastic layers by using differential quadrature method. *Journal of Sandwich Structures & Materials*, 23(1), pp. 132-173.
- [30] Ni, Y., Zhu, S., Sun, J., Tong, Z., Zhou, Z., Xu, X. and Lim, C. W., 2021. An accurate model for free vibration of porous magneto-electro-thermo-elastic functionally graded cylindrical shells subjected to multi-field coupled loadings. *Journal of Intelligent Material Systems and Structures*, 1045389X20986894.
- [31] Zhou, L., Li, M., Tang, J., Li, F. and Žur, K. K., 2021. Evaluation of performance of magneto-electro-elastic sensor subjected to thermal-moisture coupled load via CS-FEM. *Thin-Walled Structures*, 169, 108370.
- [32] Farajpour, A., Žur, K. K., Kim, J. and Reddy, J. N., 2021. Nonlinear frequency behaviour of magneto-electromechanical mass nanosensors using vibrating MEE nanoplates with multiple nanoparticles. *Composite Structures*, 260, 113458.
- [33] Sofiyev, A. H., Kuruoglu, N. and Halilov, H. M., 2010. The vibration and stability of non-homogeneous orthotropic conical shells with clamped edges subjected to uniform external pressures. *Applied mathematical modelling*, 34(7), pp.1807-1822.
- [34] Srikantamurthy, J. S., Annigeri, A. R. and Raghavendra, B. V., 2020. Free Vibration Analysis of Layered Magneto-Electro-Elastic Truncated Conical Shells. *Journal of Applied Science and Engineering*, 23(4), pp.669-676.
- [35] Srikantamurthy, J. S. and Annigeri, A. R., 2021. Free Vibration Analysis of Multiphase Magneto-Electro-Elastic Composite Conical Shells. *Indian Journal of Science and Technology*, 14(19), pp. 1525-1533.

- [36] Zarouni, E., Rad, M. J. and Tohidi, H., 2014. Free vibration analysis of fiber reinforced composite conical shells resting on Pasternak-type elastic foundation using Ritz and Galerkin methods. *International Journal of Mechanics and Materials in Design*, 10(4), pp.421-438.
- [37] Sofiyev, A. H., 2014. The combined influences of heterogeneity and elastic foundations on the nonlinear vibration of orthotropic truncated conical shells. *Composites Part B: Engineering*, 61, pp.324-339.
- [38] Asanjarani, A., Satouri, S., Alizadeh, A. and Kargarnovin, M. H., 2015. Free vibration analysis of 2D-FGM truncated conical shell resting on Winkler–Pasternak foundations based on FSDT. *Proceedings of the Institution of Mechanical Engineers, Part C: Journal of Mechanical Engineering Science*, 229(5), pp.818-839.
- [39] Wu, S., Qu, Y. and Hua, H., 2015. Free vibration of laminated orthotropic conical shell on Pasternak foundation by a domain decomposition method. *Journal of Composite Materials*, 49(1), pp.35-52.
- [40] Deniz, A., Zerín, Z. and Karaca, Z., 2016. Winkler-Pasternak foundation effect on the frequency parameter of FGM truncated conical shells in the framework of shear deformation theory. *Composites Part B: Engineering*, 104, pp.57-70.
- [41] Nguyen Dinh, D. and Nguyen, P. D., 2017. The dynamic response and vibration of functionally graded carbon nanotube-reinforced composite (FG-CNTRC) truncated conical shells resting on elastic foundations. *Materials*, 10(10), 1194.
- [42] Nguyen, P. D., Quang, V. D., Anh, V. T. T. and Duc, N. D., 2019. Nonlinear vibration of carbon nanotube reinforced composite truncated conical shells in thermal environment. *International Journal of Structural Stability and Dynamics*, 19(12), 1950158.
- [43] Chan, D. Q., Anh, V. T. T. and Duc, N. D., 2019. Vibration and nonlinear dynamic response of eccentrically stiffened functionally graded composite truncated conical shells surrounded by an elastic medium in thermal environments. *Acta Mechanica*, 230(1), pp.157-178.
- [44] Sofiyev, A. H., Mammadov, Z., Dimitri, R. and Tornabene, F., 2020. Vibration analysis of shear deformable carbon nanotubes-based functionally graded conical shells resting on elastic foundations. *Mathematical Methods in the Applied Sciences*.
- [45] Eyvazian, A., Musharavati, F., Tarlochan, F., Pasharavesh, A., Rajak, D. K., Husain, M. B. and Tran, T. N., 2020. Free vibration of FG-GPLRC conical panel on elastic foundation. *Structural Engineering and Mechanics*, 75(1), pp.1-18.
- [46] Mohammadrezazadeh, S. and Jafari, A. A., 2021. Nonlinear vibration suppression of laminated composite conical shells on elastic foundations with magnetostrictive layers. *Composite Structures*, 258, 113323.
- [47] Fu, T., Wu, X., Xiao, Z., Chen, Z. and Li, B., 2021. Analysis of vibration characteristics of FGM sandwich joined conical-conical shells surrounded by elastic foundations. *Thin-Walled Structures*, 165, 107979.
- [48] Jamalabadi, M. Y. A., Borji, P., Habibi, M. and Pelalak, R., 2021. Nonlinear vibration analysis of functionally graded GPL-RC conical panels resting on elastic medium. *Thin-Walled Structures*, 160, 107370.
- [49] Amirabadi, H., Farhatnia, F. and Civalek, Ö., 2021. Frequency response of rotating two-directional functionally graded GPL-reinforced conical shells on elastic foundation. *Journal of the Brazilian Society of Mechanical Sciences and Engineering*, 43(7), pp.1-24.
- [50] Mohammadrezazadeh, S. and Jafari, A. A., 2021. The study of the nonlinear vibration of SS and CC laminated composite conical shells on elastic foundations through an approximate method. *Proceedings of the Institution of Mechanical Engineers, Part C: Journal of Mechanical Engineering Science*, 09544062211021439.
- [51] Sofiyev, A. H. and Kuruoglu, N., 2017. Combined effects of transverse shear stresses and nonlinear elastic foundations on the nonlinear dynamic response of heterogeneous orthotropic cylindrical shells. *Composite Structures*, 166, pp.153-162.
- [52] Zhu, C., Fang, X., Liu, J. and Nie, G., 2020. Smart control of large amplitude vibration of porous piezoelectric conical sandwich panels resting on nonlinear elastic foundation. *Composite Structures*, 246, 112384.

- [53] Molla-Alipour, M., Shariyat, M. and Shaban, M., 2020. Free Vibration Analysis of Bidirectional Functionally Graded Conical/Cylindrical Shells and Annular Plates on Nonlinear Elastic Foundations, Based on a Unified Differential Transform Analytical Formulation. *Journal of Solid Mechanics*, 12(2), pp.385-400.
- [54] Civalek, Ö. and Kiracioglu, O., 2010. Free vibration analysis of Timoshenko beams by DSC method. *International Journal for Numerical Methods in Biomedical Engineering*, 26(12), pp.1890-1898.
- [55] Civalek, Ö. M. E. R., 2014. Geometrically nonlinear dynamic and static analysis of shallow spherical shell resting on two-parameters elastic foundations. *International Journal of Pressure Vessels and Piping*, 113, pp.1-9.
- [56] Mercan, K., Demir, Ç. and Civalek, Ö., 2016. Vibration analysis of FG cylindrical shells with power-law index using discrete singular convolution technique. *Curved and Layered Structures*, 3(1).
- [57] Pirbodaghi, T., Ahmadian, M. T. and Fesanghary, M., 2009. On the homotopy analysis method for non-linear vibration of beams. *Mechanics Research Communications*, 36(2), pp.143-148.
- [58] Motallebi, A. A., Poorjamshidian, M. and Sheikhi, J., 2014. Vibration analysis of a nonlinear beam under axial force by homotopy analysis method. *Journal of Solid Mechanics*, 6(3), pp.289-298.
- [59] Dastjerdi, S., Akgöz, B. and Civalek, Ö., 2020. On the effect of viscoelasticity on behavior of gyroscopes. *International Journal of Engineering Science*, 149, 103236.
- [60] Lam, K. Y. and Hua, L., 1997. Vibration analysis of a rotating truncated circular conical shell. *International Journal of Solids and Structures*, 34(17), pp.2183-2197.
- [61] Rao, S. S., 2007. *Vibration of Continuous Systems*. JOHN WILEY & SONS, INC.
- [62] Reddy, J. N., 2004. *Mechanics of laminated composite plates and shells: theory and analysis*. Second Edition, CRC Press.
- [63] Li, Y. and Zhang, J., 2013. Free vibration analysis of magneto-electro-elastic plate resting on a Pasternak foundation. *Smart materials and structures*, 23(2), 025002.
- [64] Pan, E. and Heyliger, P. R., 2002. Free vibrations of simply supported and multilayered magneto-electro-elastic plates. *Journal of Sound and Vibration*, 252(3), pp.429-442.
- [65] Harshe, G., Dougherty, J. P. and Newnham, R. E., 1993. Theoretical modelling of multilayer magneto-electric composites. *International journal of applied electromagnetics in materials*, 4(2), pp.145-145.
- [66] Nan, C. W., 1994. Magneto-electric effect in composites of piezoelectric and piezomagnetic phases. *Physical Review B*, 50(9), 6082.
- [67] Benveniste, Y., 1995. Magneto-electric effect in fibrous composites with piezoelectric and piezomagnetic phases. *Physical Review B*, 51(22), 16424.
- [68] Pan, E., 2001. Exact solution for simply supported and multilayered magneto-electro-elastic plates. *Journal of Applied Mechanics-TRANSACTIONS OF THE ASME*, 68(4), pp.608-618.
- [69] Sladek, J., Sladek, V., Krahulec, S. and Pan, E., 2013. Analyses of functionally graded plates with a magneto-electro-elastic layer. *Smart materials and structures*, 22(3), 035003.
- [70] Liu, M. F. and Chang, T. P., 2010. Closed form expression for the vibration problem of a transversely isotropic magneto-electro-elastic plate. *Journal of Applied Mechanics- TRANSACTIONS OF THE ASME*, 77(2).
- [71] Milazzo, A., 2014. Large deflection of magneto-electro-elastic laminated plates. *Applied Mathematical Modelling*, 38(5-6), pp.1737-1752.
- [72] Qatu, M. S., 2004. *Vibration of laminated shells and plates*. Elsevier.
- [73] Nayfeh, A. H. and Mook, D. T., 1995. *Nonlinear Oscillations*. John Wiley & Sons, Inc.
- [74] Irie, T., Yamada, G. and Tanaka, K., 1984. Natural frequencies of truncated conical shells. *Journal of Sound and Vibration*, 92(3), pp.447-453.
- [75] Li, F. M., Kishimoto, K. and Huang, W. H., 2009. The calculations of natural frequencies and forced vibration responses of conical shell using the Rayleigh-Ritz method. *Mechanics Research Communications*, 36(5), pp.595-602.

[76] Shah, A. G., Mahmood, T., Naeem, M. N. and Arshad, S. H., 2011. Vibration characteristics of fluid-filled cylindrical shells based on elastic foundations. *Acta mechanica*, 216(1), pp.17-28.

[77] Ramirez, F., Heyliger, P. R. and Pan, E., 2006. Discrete layer solution to free vibrations of functionally graded magneto-electro-elastic plates. *Mechanics of Advanced Materials and Structures*, 13(3), pp.249-266.